THE ASTROPHYSICAL JOURNAL, 472:145–152, 1996 November 20

THE KINEMATICS OF THE PLANETARY NEBULAE IN THE OUTER REGIONS OF NGC 4406[1]

M. ARNABOLDI AND K. C. FREEMAN
Mount Stromlo and Siding Spring Observatories, ACT 2611, Australia; magda@mso.anu.edu.au, kcf@mso.anu.edu.au

R. H. MENDEZ
Munich University Observatory, Munich 81679, Germany; mendez@usm.uni-muenchen.de

M. CAPACCIOLI
Osservatorio Astronomico di Capodimonte, Napoli 80131, Italy; capaccioli@astrna.na.astro.it

R. CIARDULLO
Kitt Peak National Observatory, National Optical Astronomy Observatories, Tucson, AZ 85726; rbc@astro.psu.edu

H. FORD
Physics and Astronomy Department, The John Hopkins University, Baltimore, MD 21218; ford@jhufos.pha.jhu.edu

O. GERHARD
Astronomical Institute, University of Basel, Basel 4102, Switzerland; gerhard@astro.unibas.ch

X. HUI
Astronomy Department, California Institute of Technology, Pasadena, CA 91125; sherry_hui@ssga.ssb.com

G. H. JACOBY
Kitt Peak National Observatory, National Optical Astronomy Observatories, Tucson, AZ 85726; jacoby@noao.edu

R. P. KUDRITZKI
Munich University Observatory, Munich 81679, Germany; kudritzki@usm.uni-muenchen.de

AND

P. J. QUINN
European Southern Observatory, Garching 85748, Germany; pjq@eso.org

Received 1996 March 7; accepted 1996 June 10

ABSTRACT

We have measured the velocities of 19 planetary nebulae (PNs) in the outer regions of the giant early-type galaxy NGC 4406 in the Virgo cluster. The kinematics of the outermost regions, at a mean radius of 142″ or 11 kpc, show rapid rotation and a low observed velocity dispersion ($\sim$166 and 96 km s^{-1}, respectively), compared with the central velocity dispersion of about 210 km s^{-1}. This supports the classification of this galaxy as an S0. Although this galaxy has a systemic velocity of -227 km s^{-1}, we found three PNs with velocities close to the mean velocity of the Virgo cluster (about 1400 km s^{-1}). We argue that these three PNs may be members of an intracluster stellar population in the Virgo cluster.

Subject headings: galaxies: clusters: individual (Virgo) — galaxies: individual (NGC 4406) — galaxies: kinematics and dynamics — planetary nebulae: general

1. INTRODUCTION

The origin and the formation of elliptical galaxies have been the subject of extensive observational and theoretical research. The discoveries of dust lanes, shells, decoupled and counterrotating cores, and polar rings (Bertola & Galletta 1978; Malin 1979; Franx & Illingworth 1988; Whitmore, McElroy, & Schweizer 1987; Capaccioli & Longo 1994) led to the conclusion that some of these objects were still in the process of formation and that the origin of ellipticals through mergers of progenitor galaxies had to be investigated. It was soon concluded that the stellar dynamical mergers of identical two-component (disk-halo) galaxies could not explain the formation of early-type galaxies because the remnants were far too diffuse to be identified with ellipticals (Ostriker 1980; Carlberg 1986; Hernquist 1992). In addition, the predicted distribution of shapes was not consistent with the observed properties of ellipticals.

Recent simulations (Barnes & Hernquist 1991; Hernquist & Barnes 1991; Barnes 1988, 1992) showed that these difficulties could be overcome if the progenitors either contained gas or were multicomponent systems with disks and compact bulges. In the first case, star formation can cause steep central densities, provided that gas can concentrate on small scale, through dissipation and the loss of angular momentum. In the second case, because of the nondissipative stellar dynamics, the inner portion of a merger remnant is constituted by the most tightly bound material from the progenitors. In a comprehensive paper, Hernquist (1993) examined the structural and kinematic properties of remnants formed by mergers of composite rotating progenitor galaxies. He showed that dynamical mergers of identical spiral galaxies can produce objects with global properties reminiscent of observed ellipticals and derived the properties which can be used to constrain the merger hypothesis observationally. He concluded that ellipticals formed by major merger events should exhibit rapid rotation in their outer regions and should display significant misalignments between their minor and rotation axes.

The segregation of angular momentum in the outer parts of elliptical galaxies has also been invoked to explain the slow rotation observed for the inner regions of most giant elliptical galaxies. This indicated that most giant ellipticals

[1] Based on observations made at the European Southern Observatory, La Silla, Chile.

appear to have an order of magnitude less angular momentum per unit mass than spiral galaxies (Bertola & Capaccioli 1975; Illingworth 1977; Binney 1978), although at that time there was no obvious theoretical reason why this should be so (Zurek et al. 1988). The possibility of testing this important prediction from observations of the integrated light is hampered by observational difficulties: the rapid falloff in surface brightness limits such measurements to within one or two effective radius r_e (Illingworth 1977; Davies et al. 1983; Franx, Illingworth, & Heckman 1989; Capaccioli et al. 1993). As a consequence, little is known about the rotation and velocity dispersion in the halos of elliptical galaxies.

Multiobject spectrographs on 4 m class telescopes allow us to study the kinematics of the halos of ellipticals by observing the faint [O III] λ5007 emission from planetary nebulae (PNs) present in those regions. For this purpose, the PNs act as test particles, providing crucial kinematical information in the halos of ellipticals. Once their velocity field is known, it is still not straightforward to determine the integrated mass because the properties of the stellar orbits in hot stellar systems are not well known. However, it is possible to place limits on the dark matter content from velocities measured at large radii. For example, Hui et al. (1995) measured radial velocities for 433 planetary nebulae in the giant elliptical NGC 5128 (Centaurus A) with the multifiber spectrograph at the Anglo-Australian telescope. These measurements extend out to about 25 kpc from the nucleus: for comparison, kinematical observations of the integrated light reach out only to about 5 kpc.

Hui et al. showed that (1) the velocity field of the PNs shows distinctive characteristics of a triaxial potential and (2) the mean rotational velocity along the major axis of Cen A rises slowly from the center of the galaxy and flattens to a value of about 100 km s^{-1} between 10 and 20 kpc from the center. The local v/σ of the stellar component is 0.5 between 5 and 10 kpc and reaches unity beyond 10 kpc. They also showed that dark matter is needed to reproduce the observed PN velocity dispersion at 25 kpc; M/L varies from 3.9 inside 5 kpc to 10 at 25 kpc.

Arnaboldi et al. (1994) applied this technique to the study of an elliptical that is less disturbed than Cen A. They used the European Southern Observatory (ESO) New Technology telescope (NTT) to study PNs in the outer halo of the cD giant elliptical NGC 1399 in the Fornax cluster. Their velocity dispersion measurements for the PNs confirm the evidence from the kinematics of the globular cluster system (Grillmair et al. 1994) that the integrated M/L_B ratio in NGC 1399 is at least 80 within 20 kpc. Moreover, the 37 PN velocities which they measured in the outer region of NGC 1399 have shown the presence of rapid rotation of 290 km s^{-1}, at a distance of 24 kpc from the center along the P.A. $= -35°$. So it seems that the stellar dynamics of NGC 1399 is similar to that in Centaurus A: the inner regions are slowly rotating and the stellar halo rotates rapidly, so the outer regions contain a large amount of angular momentum.

NGC 1399 is a cD galaxy which appears to merge into the Fornax cluster, structurally and kinematically (Grillmair et al. 1994): its M/L_B ratio of at least 80 within 20 kpc approaches the value of a cluster M/L ratio and that the dynamics of the PNs at large distances from the center of NGC 1399 is driven more by the gravitational potential of the cluster than by that of the galaxy itself. In this paper, we would like to extend this study to a normal giant early-type galaxy to see if it also shows the high angular momentum observed in the outer regions ($r > 2r_e$) of Centaurus A and NGC 1399 and therefore may have a similar formation history. We have chosen to study the non-cD giant NGC 4406 in the Virgo cluster. This galaxy has a kinematically distinct core (Bender 1988; Fried & Illingworth 1994) and shows modest minor axis rotation in its inner regions (Wagner, Bender, & Moellenhoff 1988; Franx, Illingworth, & Heckman 1989) but is otherwise a typical giant early-type E/S0 galaxy with little rotation in its central regions ($v/\sigma = 0.07$) and a velocity dispersion σ of about 200 km s^{-1} inside 50″ (Fried & Illingworth 1994). However, we note for later reference that the RSA classification (Sandage & Tammann 1981) for NGC 4406 is S0$_1$(3)/E3. Jacoby, Ciardullo, & Ford (1990) have discovered 141 PNs in this galaxy, and we have used these PNs to study the kinematics of its outer regions out to a radius of about $3r_e$.

In § 2 we describe the observations and the instrumental set-up. We discuss the data reduction and the errors in our velocity measurements in § 3, the results in § 4, and the conclusions are derived in § 5.

2. OBSERVATIONS

We acquired spectra for 66 PNs in NGC 4406 with the ESO NTT at La Silla on three nights (1995 April 30 to May 2). We used the EMMI spectrograph in the red imaging and low dispersion mode with multiobject spectra (MOS) masks, the f/5.3 camera and the TEK2048 CCD (24 μm = 0.″26 pixel^{-1}), and the No. 5 grism: the wavelength range is 4120–6330 Å, with a dispersion of 1.30 Å pixel^{-1}. The only emission line visible in the spectra of these faint PNs is [O III] λ5007, so a filter with a central wavelength $\lambda_c =$ 5050 Å and FWHM = 500 Å was used in front of the grism to reduce the wavelength range of each spectrum. This allowed us to increase the number of slitlets in each MOS mask and also to get enough emission lines from the calibration exposures for an accurate wavelength calibration. The size of the slitlets punched in the MOS masks is 1″ × 7″, which corresponds to 3.84 × 27 pixel at the CCD.

2.1. *Production of the MOS Plates*

Astrometry and [O III] photometry for 141 PNs in NGC 4406 came from Jacoby et al. (1990). Arnaboldi et al. (1994) discuss at length the impossibility of using precise (α,δ) PN positions directly to produce the MOS plates, since an accurate map of the distortion in the NTT focal plane (NTT-fp) is not available. The standard method to produce MOS plates requires that the objects are identified on (NTT + EMMI) images, with the same set-up as the one used to obtain the spectra. Our nonstandard method uses images from other telescopes; it is discussed in length by Arnaboldi et al. (1994) and will be only briefly summarized here.

The 141 PNs in NGC 4406 were initially identified with the *on-band/off-band* technique on two 4′ × 4′ fields, using images obtained at the Kitt Peak 4 m telescope (KPNO) with the TI2 CCD (0.″3 pixel^{-1}). The east field is centered at $\alpha(1950) = 12^h23^m47^s.7$, $\delta(1950) = +13°12'43''$, the west field at $\alpha(1950) = 12^h23^m32^s.0$, $\delta(1950) = +13°14'01''$, both off-center with respect to the nucleus of NGC 4406. We were able to map the two combined KPNO images into a unique NTT field (10′ × 10′) centered on NGC 4406, using a 5 minute V-band exposure, which George Miley kindly obtained for us. Each 4′ × 4′ KPNO image was trans-

formed to a corresponding 10′ × 10′ NTT frame, using up to 40 stars which were in common between the KPNO image and the corresponding area in the NTT frame.[2] It turned out that in the east KPNO field there was a lack of stars in one corner of the image, while in the west KPNO field the reference stars were homogeneously distributed.

The two KPNO frames, transformed into the NTT-fp, were subsequently combined to obtain a single image, from which the PNs (x, y) positions were derived to produce the MOS masks. The combined KPNO image of NGC 4406 now covered a 10′ × 10′ field with PNs present over a large part of the image. The punching area for the MOS masks is 5′ × 8′, and three MOS masks were made to include the maximum number of PNs. One mask was offset 134″ east of the nucleus of NGC 4406, the second mask was centered on the nucleus, and the third mask was offset 134″ west; the central and offset masks overlap by 2.′75 × 8′, and there is no overlap between the two offset masks. In each mask, two slitlets were punched at positions corresponding to reference stars in the NGC 4406 field which we used to monitor the telescope pointing. The east mask contained 34 slitlets corresponding to 32 PNs plus the two reference stars, the central mask contained 44 slitlets (42 PNs and the two stars), and the west mask contained 36 slitlets (34 PNs plus two stars). The east and central masks had seven PNs in common, eight PNs were in common between the west and central masks, and the total number of PNs included by the three MOS plates is 93. Unfortunately our observations were affected by a systematic scale error in the EMOS package, which was later discovered by the ESO staff in July of 1995. This effect caused the distance between punched slits to be 1.005 times larger than the distance requested through the EMOS MIDAS context: therefore some PNs emissions were not detected because of the systematic error in the position of the corresponding punched slitlet.

2.2. *The Observations*

Spectra were taken for the east mask on 1995 May 1–2, with a total integration time of 3.3 hr and an average seeing of 1.″2. Spectra for the west field were acquired on May 2, with an average seeing of 1.″2 and a total integration time of 2.7 hr. One night was lost because of bad weather, and the central mask could not be used. Our time was scheduled somewhat late in the season, which restricted the actual observing time. Therefore the success of the observations depended even more than usual on having the best possible image quality, so we performed image analysis twice a night and regularly checked the focus.

3. DATA REDUCTION

Flat-field exposures for the two MOS masks (east and west) were taken with the internal lamp, the grism, and the interference filter. The bias frames were flat and constant throughout each night, and the dark current was negligible.

Before combining all the frames for each mask, we carefully checked for any shift in the wavelength direction (x) and y which could possibly effect our velocity measurements. For the east mask, a maximum shift of $\Delta x = 0.55$ pixel, constant for all the slitlets, was detected from one calibration lamp frame to the other. For the west mask, the maximum shift $\Delta x = 0.4$ pixel, again constant throughout the mask, was detected. No y shift was detected for either mask. Each PN frame was then corrected for its Δx shift, and the frames for each mask were combined. After combining, the two resulting MOS frames appeared free of cosmic rays. Then the two-dimensional spectra of each PN were extracted and wavelength calibrated using the corresponding He-Ar spectrum in the combined calibration frames.

At this point we derived the sky background for each two-dimensional PN spectrum by fitting a Legendre polynomial to the collapsed and normalized two-dimensional spectrum. The fitted sky background was subtracted from each individual spectrum. The rows where the [O III] emission appears were averaged, and the redshifted λ5007 line was measured using a Gaussian fit. Spectra were extracted for 66 PNs, and we were able to measure the velocities for 19 PNs.

3.1. *Errors of the Velocity Measurements*

Arnaboldi et al. (1994) were able to determine an external error of ± 73 km s^{-1} for a single velocity measurement; their observations were made with a camera/CCD combination that gave less resolution than the system used for the NGC 4406 observations. This error, which comes from (1) the wavelength calibration, (2) photon noise, and (3) astrometric errors, was derived from comparison of velocities of PNs common to the two masks used for their observations of NGC 1399. For the observations of NGC 4406 reported here, the loss of one night to bad weather made it impossible for us to observe PNs with all three MOS masks; we do not have PNs in common to our east and west masks, and we cannot determine directly the external errors of our velocity measurements. In the following discussion, we attempt to make a realistic estimate of the velocity errors for the NGC 4406 PNs.

In this relatively low resolution multiobject spectroscopy, the finite width of the slitlets is a significant source of error in the velocity measurements. If the PNs are not precisely at the slitlet centers (in the direction of the dispersion), this can generate velocity errors of up to 90 km s^{-1} at worst (i.e., maximum displacement and excellent seeing). Pointing errors, which affect the velocities of all of our PNs in this way, are not of major concern: they affect only the mean velocity of the set of PNs. However, the velocities of individual PNs can be affected by random offsets of the object from the slit center, generated, for example, by local errors in the geometric transformations from the KPNO to the NTT-fp, and by random errors produced by the slitlet punching machine itself. We refer to these random position errors collectively as "astrometric" errors. From our geometric transformation fits, we know that errors in the positions of the stars in the NTT-fp are small: the upper limit is 0.26 pixel or 20 km s^{-1}. We must now estimate the errors in the slitlet positions introduced during the punching of the MOS masks. We do this by evaluating the contribution to the errors from the wavelength calibration and photon noise and compare this contribution to the total (external) errors derived earlier by Arnaboldi et al. (1994).

The wavelength range of our two-dimensional PN spectra is 500 Å, centered on 5050 Å, so we detect the weak [N I] auroral doublet (from the sky) near 5199.6 Å. We

[2] With hindsight, the best method to handle the geometrical distortions from the 4′ × 4′ KPNO frames to the NTT-fp would have been to obtain two 5 minute V-band NTT exposures, at the same centers as the KPNO frames, and then derive the geometrical distortion map for each of the KPNO-NTT frames independently.

determine the apparent wavelength λ_c for these auroral lines for each of our slitlets in the same way we use to derive the wavelength for the PN [O III] emission, by averaging over three rows (or 0".78) and deriving the wavelength via a Gaussian fit. Our wavelength calibration is derived from four He-Ar arc lamp emission lines: 4921.9, 5015.7, 5047.7, and 5187.7 Å. Therefore the estimates of λ_c for the [N I] doublet give an upper limit on the error from the wavelength calibration and photon noise, because the [N I] lines lie outside the region spanned by the arc lines.

For each two-dimensional slitlet spectrum, we determine nine sets of λ_c values, each coming from the average of three rows, and then the standard deviation σ_3 of these nine λ_c values. We then compute the mean values $\bar{\lambda}_c$, $\bar{\sigma}_3$, and σ_{λ_c} over all the slitlets in the east and west masks, respectively. For the east mask, we obtain $\bar{\lambda}_c = 5199.75$ Å, $\bar{\sigma}_3 = 0.88$ Å $= 53$ km s^{-1}, and $\sigma_{\lambda_c} = 0.37$ Å $= 21$ km s^{-1}. For the west mask the corresponding values are $\bar{\lambda}_c = 5199.10$ Å, $\bar{\sigma}_3 = 0.60$ Å $= 36$ km s^{-1}, and $\sigma_{\lambda_c} = 0.31$ Å $= 18$ km s^{-1}. The average $\bar{\sigma}_3$ over the east and west masks gives us an upper limit on the errors due to the wavelength calibration and photon noise of 0.74 Å $= 0.57$ pixel $= 44$ km s^{-1}. We note that the strength of the [N I] lines is a little stronger than, but comparable to, the typical strength of the PN emission lines.

For the observations described by Arnaboldi et al. (1994), the calibration errors were almost identical in pixel units to those for our NGC 4406 observations, but the instrumental dispersion was different: 1 pixel = 1.75 Å. Their errors due to wavelength calibration and photon noise corresponded to 1.00 Å $= 60$ km s^{-1}. Their total external error (wavelength calibration + photon noise + astrometric error) was $\sigma_{\rm total} = 73$ km s^{-1}: the contribution from the astrometric only is then $\sigma_{\rm ast} = 42$ km s^{-1} $= 0.40$ pixel.

The astrometric error $\sigma_{\rm ast} = 0.40$ pixel for the Arnaboldi et al. observations corresponds to an error of 26 μm in the NTT-fp.[3] We now assume that the astrometric errors in microns in the NTT-fp were the same in 1993 November and 1995 May and derive the astrometric error for the NGC 4406 observations. With a reduction factor of 2.03 for the Tek2048 CCD, the astrometric error of 26 μm in the NTT-fp corresponds to 13 μm at the Tek CCD, which is equal to 0.54 pixel = 0.70 Å = 42 km s^{-1}. Our estimate of the total error for the NGC 4406 velocity measurements (44 km s^{-1} from the calibration and photon errors, and 42 km s^{-1} from the astrometric contribution) is then 61 km s^{-1}.

The data themselves provide a rough upper limit to the likely observational errors. Anticipating the results of the next section, we see that the outer PNs of NGC 4406, at a mean radius of 142", show rapid rotation of about 166 km s^{-1} and a relatively low velocity dispersion of 96 km s^{-1}. The observed velocity dispersion of objects in a rotating system comes from three sources: the line-of-sight contribution from the rotation field itself, the true velocity dispersion of the objects about the rotation field, and the measurement errors. Assuming that the true rotation curve is flat, we estimate from simple arguments that the rotation field contributes about 35 km s^{-1} to the velocity dispersion. The true velocity dispersion in the outer regions of this apparently S0 galaxy is unlikely to be less than the velocity dispersion of the old Galactic disk near the Sun: we take this to be 35 km s^{-1} in the mean. Assuming that the error contributions add quadratically, the observed velocity dispersion of 96 km s^{-1} suggests that the measuring error is probably less than 80 km s^{-1}. This is certainly consistent with the estimate of the total measuring error given in the previous paragraph.

Because we observed NGC 4406 at larger than usual air masses and our exposure times were restricted by the late scheduling of the observations, the signal-to-noise ratio of our PNs [O III] λ5007 detections is mostly at only the 2 σ level. To verify the reality of our detections, we looked for the weak [O III] λ4959 emission from the PNs by averaging over all of the candidate PN emission spectra, after shifting the spectra in wavelength so that the [O III] λ5007 emission lines were all at the same apparent λ. The result was positive: we could detect a faint emission at 4959 Å, with the expected flux.

4. RESULTS

With the NTT and the EMMI + MOS facility, we have been able to measure velocities for 19 PNs lying in the outer parts of the giant galaxy NGC 4406 between 3 and 19 kpc from the center. This region extend well beyond the limits for the integrated light velocity measurements of $1r_e = 91" = 7$ kpc. Of the 19 PNs, 16 have velocities near the expected redshift $v_{\rm sys} = -227$ km s^{-1} of NGC 4406: a two-dimensional linear fit to the data[4] of the form $v = ax + by + c$ to the velocities and (x, y) positions of these PNs gives a mean velocity $\bar{v} = -214$ km s^{-1} and a strong velocity gradient of 1.19 ± 0.33 km s^{-1} arcsec^{-1} along P.A. $= 111°.5 \pm 28°$, very near to the galaxy photometric major axis. The observed rotation has the same sense as the rotation derived from the integrated light observations of Fried & Illingworth (1994). This maximum velocity gradient corresponds to a velocity of 300 km s^{-1} at 19 kpc. The rotation can be clearly seen in Figure 1*a*, which shows the PN positions in the NGC 4406 field: different symbols are used for velocities above and below $\bar{v}$. Figure 1*b* shows the observed velocities $(v - \bar{v})$ against the linear coordinate $z1$ along the direction of maximum gradient: the distribution of the observed velocities clearly shows the rotation of the outer regions. Once the linear rotation field is subtracted from the observed PN velocities, there is no residual velocity gradient and the dispersion of the residual velocities $\Delta v = v_{\rm obs} - v_{\rm rot}$ is $\sigma_{\Delta v} = 162.3$ km s^{-1}. The histogram of the Δv values shown in Figure 2 is fitted by a Gaussian distribution with $\Delta v_{\rm mean} = 0$ km s^{-1} and the above $\sigma_{\Delta v}$.

Comparing the v/σ values from the inner integrated light measurements with the v/σ values for the 16 PNs, we see that v/σ increases from 0.07 inside 60" (Fried & Illingworth 1994) to 0.92 at 120": Figure 3*a* shows the integrated light measurements of velocity dispersion against the logarithm of the radius, together with the PN velocity dispersion and the linear rotation field for comparison. The rotation becomes dynamically significant for $r > 2'$. Figure 3*b* shows the radial distribution of Δv. It appears that the velocity distribution of the PNs is not isothermal: the scatter of Δv decreases at radii $r > 100"$. If we partition our data in two subsamples with $r < \bar{r}$ and $r > \bar{r}$, where $\bar{r} = 120"$ is the

[3] The reduction factor with the Loral CCD was 4.38.

[4] We choose to fit a linear rotation law rather than a flat rotation curve, because the linear law is probably more appropriate to the mean rotation of this relatively hot stellar system.

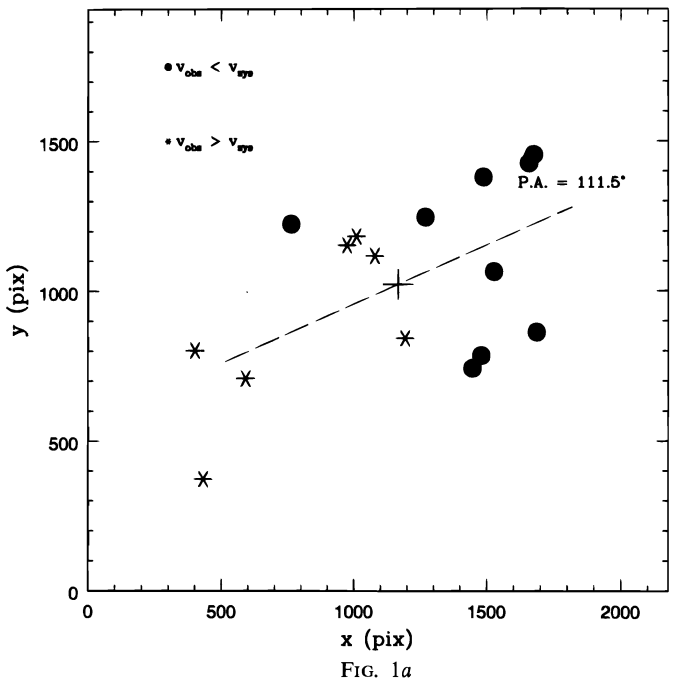

FIG. 1a

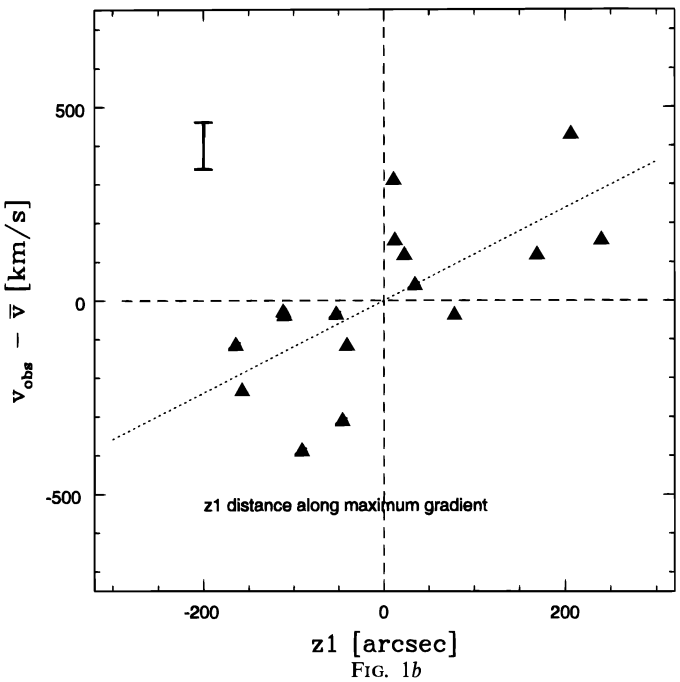

FIG. 1b

FIG. 1.—(*a*) Positions of the PNs in the NGC 4406 field; north is up, east to the left. Filled circles indicate velocities below the mean value $\bar{v} = -214$ km s^{-1}, stars indicate velocities above $\bar{v}$. The dashed line shows the direction of the maximum velocity gradient. (*b*) $v_{obs} - \bar{v}$ vs. $z1$, where $z1$ is the linear coordinate along the direction $z1$ of strongest velocity gradient. The rotation is evident: the dashed line indicates the linear fit to the data, the error bar in the upper left corner indicates $\pm 1\,\sigma$ error on each single velocity measurement.

average radius of the PN sample, we find that the mean radius of the inner subsample (nine objects) is 66″ and $\sigma_{\Delta v1} = 209 \pm 49$ km s^{-1}, and for the outer subsample (seven objects) the corresponding quantities are 142″ and 96 ± 26 km s^{-1}. The kinematics of the outer PNs with $r > 100''$ (large rotation and lower velocity dispersion) are disklike and support the RSA classification of $S0_1$. Inspection of a fairly deep UK-Schmidt image of the Virgo cluster further supports this classification.

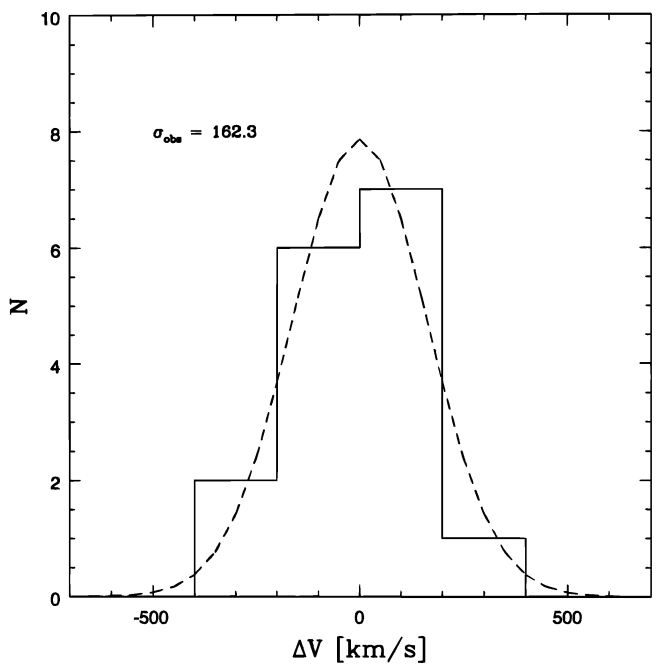

FIG. 2.—Histogram of Δv in bins of 200 km s^{-1}. The distribution is well approximated by a Gaussian (*dashed line*) with $\Delta v_{mean} = 0$ km s^{-1} and a $\sigma = 162.3$ km s^{-1}; the value corrected for the velocity resolution is 150.4 km s^{-1}. No systematic residuals are left after the subtraction of the rotation velocity component.

The velocities of the PNs imply a total mass in NGC 4406 of about $4 \times 10^{11}\,M_\odot$ within 19 kpc, corresponding to an $M/L_B = 13\,M_\odot/L_\odot$, very similar to that observed for NGC 5128 at the same distances from its center.

Could the systematic scale error in the production of the EMOS masks produce a false linear gradient in our sample of observed PN radial velocity? This unwelcome possibility is real: the systematic scale error could indeed introduce a fake linear gradient in the velocities, even when we had punched two slitlets at fiducial star positions to verify the pointing. This effect would introduce on average a systematic blueshift in the east mask, and a systematic redshift in the west mask, opposite to the linear gradient we detected in the PNs velocities. Therefore we can conclude that the rotation we observed is real and that it is a lower limit.

5. INTRACLUSTER PLANETARY NEBULAE CANDIDATES

In addition to the 16 PNs with redshifts near the redshift of NGC 4406 (−227 km s^{-1}), in the west field we also detected three objects with emission at a different redshift. One of these three emissions was observed to be very near to the [O I] sky emission line at λ5577 that was leaking through our filter from a nearby slit. We did the sky subtraction, which worked very well, and the emission was still there, with all the characteristics of those PNs emissions previously identified for NGC 4406. If we assume that this emission also corresponds to [O III] λ5007, then these three PNs have redshifts 1729 km s^{-1}, 1651 km s^{-1}, and 1340 km s^{-1}.

Their mean redshift (1573 km s^{-1}) is consistent with the mean redshift for the Virgo cluster; their rms dispersion is 206 km s^{-1}. Why did Jacoby et al. (1990) find these high-

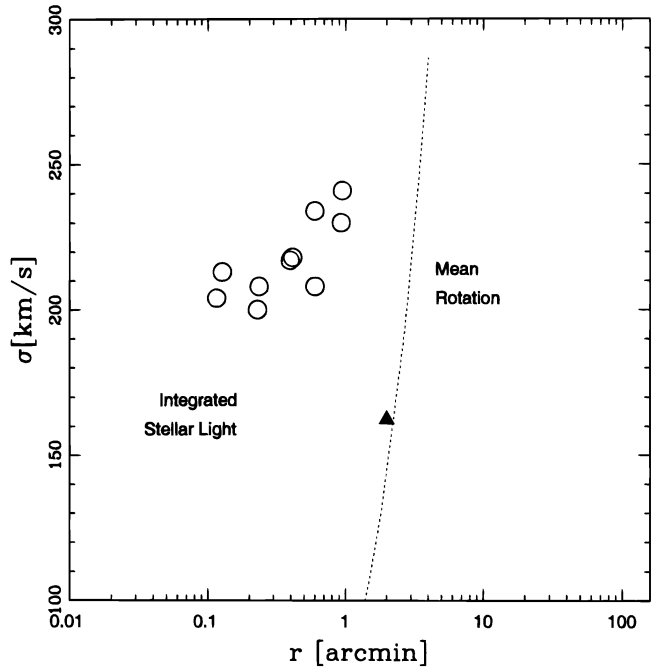

FIG. 3a

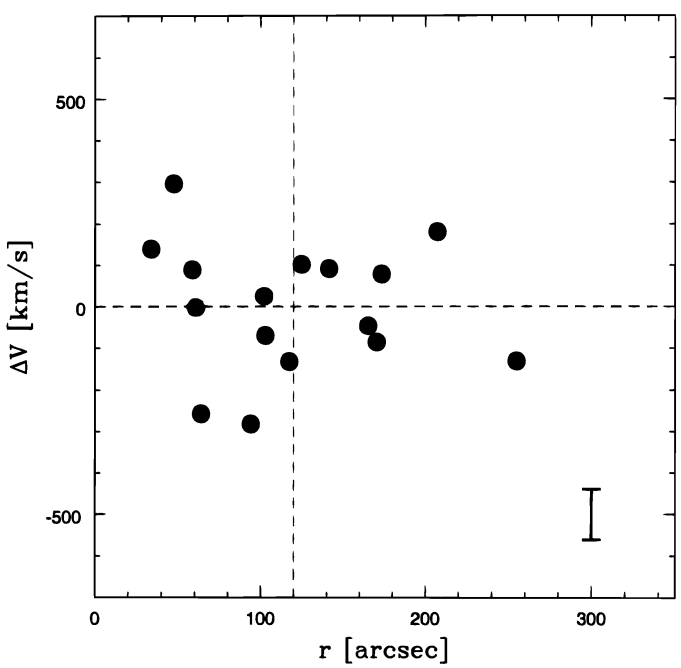

FIG. 3b

FIG. 3.—(*a*) Velocity dispersion σ vs. log r for (1) integrated light of NGC 4406 from Fried & Illingworth and (2) our PN velocity measurements (*solid triangle*). The dotted curve shows the rotational velocity for our solid body rotation fit to the velocities of the PNs. (*b*) Δv vs. radius r: the residual velocity data appear to be less scattered at larger radii that in the central regions. The dashed line indicates the average radius of the distribution, at $\bar{r} = 120''$, the error bar in the right lower corner indicates $\pm 1\,\sigma$ error on each single velocity measurement.

velocity PNs in their survey, using an [O III] filter designed to discover PNs in NGC 4406 ($v_{sys} = -227$ km s^{-1})? For their on-band images, they used a filter centered at 4998 Å with FWHM = 30 Å. By chance, this filter would include the [O III] λ4959 line at the velocity of the Virgo cluster, and we suggest that they detected the 4959 Å line in these three higher velocity PNs. If this is correct, then we would expect these PNs to be among the fainter objects in the Jacoby et al. (1990) catalog. This is indeed so; their average "m_{5007}" magnitude is 27.5, compared to the mean $m_{5007} = 26.9$ for the NGC 4406 PNs, which we were able to detect spectroscopically. We would like to explore the possibility that these three PNs are intracluster PNs. In what follows, we will discuss only the PNs discovered in the West field. As stressed in § 2.1, the reference stars from the KPNO-NTT coordinate transformation of the east field were not homogeneously distributed, and this affected the production of the east MOS mask, resulting in a low detection rate for PNs in this field.

The goal of this discussion is to compare the surface density of (1) possible intracluster matter associated with these three PNs with (2) the total surface density of Virgo cluster matter at the location of NGC 4406. From Jacoby et al. (1990), the area of their images surveyed for PN include only the regions fainter than the $\mu_V = 21.52$ mag arcsec^{-2} isophote, which has a major axis of 80″. The total area of this surveyed region in their west field is 13.5 arcmin^2, and its total luminosity is $V = 11.25$ or $6.7 \times 10^9\ L_{\odot,V}$.

First, we estimate the galactic mass in this surveyed region, using the Jeans equations and the following assumptions and simplifying approximations: (1) The distribution of the total mass in NGC 4406 is spherical. (2) The stellar velocity dispersion is isotropic, constant at $\sigma = 210$ km s^{-1} for radius $r < 80''$, and constant at $\sigma = 96$ km s^{-1} for $r > 80''$. (3) The stellar surface density distribution $\Sigma(r)$ is a power law, $\Sigma(r) \propto r^{-n}$, where $n = 1.18$ for $r < 80''$ and $n = 1.60$ for $r > 80''$, following the surface brightness distribution (Peletier et al. 1990). (4) The angle between the rotation vector and the line of sight is 58°, derived from the observed ellipticity and assuming that the intrinsic ellipticity is 0.3 (the estimate does not depend strongly on this assumption), so the intrinsic mean rotational velocity is $1.40 \times r$ (arcseconds) km s^{-1}. Integrating over the survey area of the west field then gives a projected total mass of $7.7 \times 10^{10}\ M_\odot$ and a projected luminosity of $6.7 \times 10^9\ L_{\odot,V}$, so the M/L_V ratio for the survey region is 11. In this west field, we detected spectroscopically 10 galactic PNs: this corresponds to one PN for each $7.7 \times 10^9\ M_\odot$ or $6.7 \times 10^8\ L_{\odot,V}$ of galactic matter. Then the detection of three possible intracluster PNs would suggest the presence of $2.3 \times 10^{10}\ M_\odot$ of galaxy-like intracluster material in the 13.5 arcmin^2 region surveyed. The associated surface density of this material is then $82\ M_\odot$ pc^{-2}.

We can compare this with the estimated *total* surface density of Virgo cluster matter near NGC 4406, derived from the velocity dispersion of the Virgo cluster and an estimate of its radial scale. We adopt $\sigma_{\rm cluster} = 800$ km s^{-1} and a cluster core radius of $r_0 = 0.5$ Mpc, and assume that the mass distribution in the Virgo cluster follows a King law (Binggeli et al. 1987). Then the estimated surface mass density of the Virgo cluster at the distance of M86 from the cluster center is

$$\Sigma(0.26r_0) = 1.85\rho_0 r_0 = 1.85\,\frac{9\sigma^2_{\rm cluster}}{4\pi G r_0} = 392\ M_\odot\ \mathrm{pc}^{-2}\ .$$

This total surface density is of similar order of magnitude, although larger, than the estimated surface density of intracluster material associated with the three PNs. If we compute the average density of the Virgo cluster over the

entire cluster, assuming an isothermal mass distribution with the above $\sigma_{\rm cluster}$ and a cluster radius of $r_{\rm cluster} = 1$ Mpc, we find $\bar{\Sigma} = 94\ M_\odot\ {\rm pc}^{-2}$, in very good agreement with the surface mass density derived from the three PNs. It is tempting to speculate that much of the mass of the Virgo cluster is made up of a mixture of stars and dark matter, similar to that found in the giant galaxies themselves.

Why is the rms dispersion of the intracluster PNs sample only 206 km s^{-1}? This is related to the way that we believe these PNs were originally discovered in the Jacoby et al. survey. Their velocity must be larger than $v \sim 1400$ km s^{-1}, so that the [O III] λ4959 emission is redshifted into the wavelength range of the narrow filter used by Jacoby et al. Therefore only the high-velocity tail of the intracluster PNs sample could be detected. If we assume that the intracluster PN velocities are distributed like a Gaussian with $\sigma = 800$ km s^{-1} and $v_0 = 1400$ km s^{-1}, then our intracluster PN sample is incomplete by at least a factor 2. Although this incompleteness would affect some of the order-of-magnitude estimates given above and below, we choose to ignore it here because of the large uncertainties in many of the parameters involved.

Could these three PNs belong to M84, which is the nearest giant elliptical with positive redshift ($v_{\rm sys} = 1000$ km s^{-1})? Using the luminosity profile of M84 (Peletier et al. 1990), we can evaluate its total luminosity in the surveyed area of the west field of NGC 4406. We recall that one galactic PN in NGC 4406 corresponds to $6.7 \times 10^8\ L_{\odot,1V}$ of galactic luminosity. We assume the same ratio for M84. If the three PNs belong to M84, then we would expect it to contribute a luminosity of $2 \times 10^9\ L_{\odot,V}$ in the surveyed area. From the luminosity profile of M84, the surface brightness at the center of the west field is $\mu_V = 30.3$, so the total light contributed by M84 in this area is then only $7.8 \times 10^6\ L_{\odot,V}$, which is about 250 times smaller than required. The possibility that these three PNs belong to M84 seems remote.

We can also estimate the contribution of this possible intracluster stellar population to the total surface brightness of the Virgo cluster. With one PN in NGC 4406 corresponding to $6.7 \times 10^8\ L_{\odot,V}$ of galactic light, the presence of three intracluster PNs in the 13.5 arcmin^2 survey field implies a surface brightness of about $7\ L_{\odot,V}\ {\rm pc}^{-2}$ (with very large uncertainties). We compare this with the surface brightness from all galaxies, estimated as $0.7\ L_{\odot,B}\ {\rm pc}^{-2}$ at the center of the Virgo cluster (Binggeli et al. 1987). It appears that this possible intracluster population could contribute very significantly to the diffuse light in the Virgo cluster. This conclusion is in agreement with the recent findings by Bernstein et al. (1995), who studied the luminosity function of the Coma cluster core for $-25 < M_R < -9.4$ and its diffuse stellar light. They found that the flux of the diffuse starlight surrounding NGC 4874 is comparable to the total amount in galaxies of any size within the central 100 kpc. The discovery of a Type Ia supernovae, with a low-mass white dwarf progenitor (Smith 1981; Capaccioli et al. 1983; B. Schmidt 1996, private communication) in the region between M86, M84, and NGC 4387 gives further evidence for the presence of a stellar intracluster population in this region of the Virgo cluster. If we compute (1) the total luminosity of the intracluster population, based on our PN estimates, in an area of 0.°5 centered on NGC 4406, and (2) adopt the Type Ia supernovae frequency for an E/S0 stellar population, i.e., $0.98\ h^2/(10^{10}\ L_{\odot,B}\ 100\ {\rm yr})$ (van den Bergh & Tammann 1991), we would expect to see one supernovae every 20–50 yr. This is only an indicative number, given the large uncertainties of the quantities used. No systematic supernovae searches have been done so far in the Virgo cluster field: the region around M86 should be a high priority one for such studies.

The hypothesis that these three PNs belongs to the intracluster medium of the Virgo cluster appears viable at this stage, and we consider it to be an exciting possibility which must be further investigated. Our observations suggest this possibility but are far from conclusive. They give us only a hint that must be further tested: better, more extended PNs surveys are needed for M86 and better signal-to-noise detections must be obtained to verify this hypothesis. We also examined a very deep exposure of the Virgo cluster around M86 kindly given to us by David Malin; see Figure 4 (Plate 5): an extended envelope of diffuse stellar light surrounds M86 and other eight Virgo cluster members. Furthermore, this very deep image shows that the outer regions of M84 (= NGC 4374) are unperturbed: there is no evidence of physical interaction with M86. We have also checked the observed redshift of the eight galaxies nearest to M86 (the largest object in the image center) : NGC 4402, NGC 4374, NGC 4387, NGC 4388, NGC 4413, NGC 4425, NGC 4435, and NGC 4435. They are 232, 1000, 561, 2524, 102, 1883, 71, and 800 km s^{-1}, respectively. The two galaxies with highest redshift (NGC 4388 and NGC 4425) lie quite far from M86, and it seems very unlikely that those three PNs may belong to any of these systems. We note the presence of an X-ray tail and H I emission in the same region as the PNs but without any obvious optical counterparts (Bregman & Roberts 1990).

6. CONCLUSIONS

The ESO NTT with EMMI is a very versatile instrument with which we can acquire spectra of distant extragalactic PNs with [O III] λ5007 fluxes below about 3×10^{-17} ergs cm^{-2} s^{-1}. We have used this system in multislit mode to measure radial velocities of a sample of PNs in the outer regions of NGC 4406, in the Virgo cluster. Despite the limited statistics of our PNs radial velocity sample, due to a somewhat difficult observing run, the velocity field is showing for the first time the kinematics of the outer region of this very interesting object. The PNs radial velocities show that this object is an S0, as previously described in the RSA catalog, with the outer halo supported by rotation. The direction of maximum velocity gradient among the PNs in NGC 4406 is very near to the photometric major axis at P.A. = 123°, and the velocity dispersion decreases from 210 km s^{-1} in the center to 96 km s^{-1} in the outer region. Because of the poor statistics of this sample more observations must be done to confirm the results obtained so far. In particular, the Jacoby et al. survey was limited to an area along the galaxy photometric major axis: a more homogeneous survey should be done.

In addition to the 16 PNs observed at the redshift of NGC 4406, we detected three PNs whose emissions, if interpreted as [O III] λ5007, are at the redshift of the Virgo cluster. We suggest that these three PNs might belong to an intracluster stellar population. This working hypothesis predicts (1) a surface mass density for the intracluster matter in rough agreement with the dynamics of the Virgo cluster and (2) a substantial contribution to the diffuse light in the cluster from the intracluster stellar population. The latter

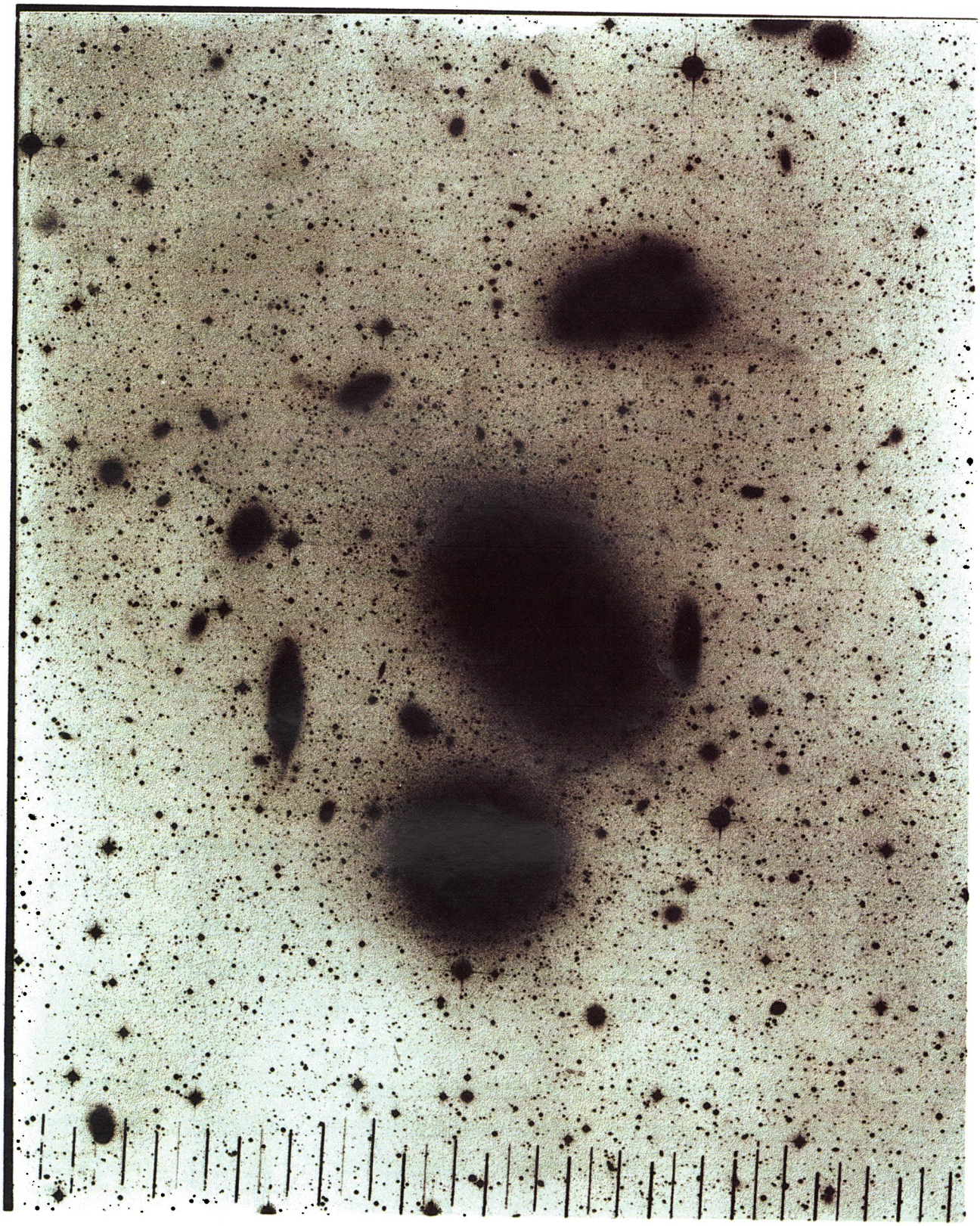

FIG. 4.—Negative of a deep image of the Virgo cluster in the region of M86. East is up, and north is on the right. The image was obtained from six UKST plates for a total integration time of 450 minutes with the emulsion IIIa-J and the GG 395 filter. The area covered by the image is one degree squared centered on NGC 4406 (the largest object near the center of the image). The other brightest galaxies visible in the plate are (clockwise from NGC 4406): NGC 4402 (the small galaxy near the shell of NGC 4406), NGC 4374 (M84, the second largest object in the picture), NGC 4387, NGC 4388, NGC 4413, NGC 4425, NGC 4438, and NGC 4435.

result is in agreement with a recent study of the diffuse stellar light in the core of the Coma cluster: Bernstein et al. (1995) find that the total light flux from the diffuse component is comparable to the total amount in galaxies. We consider this to be a very interesting hypothesis which may open a new way of studying the galaxy-cluster interactions.

The authors would like to thank George Miley for kindly obtaining the 5 minute V-band exposure of the NGC 4406 field, which was essential for the MOS plate production and for the success of the observations. The authors are grateful to the NTT team and the ESO staff at La Silla and in Santiago for their help and support before and during the observations. We are grateful to Craig Sarazin for drawing our attention to the X-ray observations of NGC 4406 and Brian Schmidt for very helpful discussions on Type Ia supernovae and their absolute frequencies. Finally the authors would like to thank David Malin for kindly lending us the deep image of the Virgo cluster around M86, and Jeremy Mould for his comments on the incompleteness of the intracluster PN sample. R. H. M. acknowledges support by the Deutsche Forschungsgemeinschaft through grant SFB 375. This research has made use of the NASA/IPAC Extragalactic Database (NED), which is operated by the Jet propulsion Laboratory, Caltech, under contract with the National Aeronautic and Space Administration.

REFERENCES

Arnaboldi, M., Freeman, K. C., Hui, X., Capaccioli, M., & Ford, H. 1994, ESO Messenger, 76, 40
Barnes, J. E. 1988, ApJ, 331, 699
———. 1992, ApJ, 393, 84
Barnes, J. E., & Hernquist, L. 1991, ApJ, 370, L65
Bertola, F., & Capaccioli, M. 1975, ApJ, 200, 439
Bertola, F., & Galletta, G. 1978, ApJ, 226, L115
Bender, R. 1988, A&A, 202, L5
Bernstein, G. M., Nichol, R. C., Tyson, J. A., Ulmer, M. P., & Wittman, D. 1995, AJ, 110, 1507
Binggeli, B., Tammann, G. A., & Sandage, A. 1987, AJ, 94, 251
Binney, J. J. 1978, A&AS, 183, 501
Bregman, J. N., & Roberts, M. S. 1990, ApJ, 362, 468
Capaccioli, M., Cappellaro, E., Held, E. V., & Vietri, M. 1993, A&A, 274, 69
Capaccioli, M., Davoust, E., Lelièvre, G., & Nieto J. L. 1983, in IAU Colloq. 78, Astronomy with Schmidt-Type Telescopes (Dordrecht: Reidel), 379
Capaccioli, M., & Longo, G. 1994, A&A Rev., 5, 293
Carlberg, R. G. 1986, ApJ, 310, 593
Davies, R. L., Efstathiou, G., Fall, S. M., Illingworth, G. D., & Schechter, P. L. 1983, ApJ, 266, 41
Franx, M., & Illingworth, G. D. 1988, ApJ, 327, L55
Franx, M., Illingworth, G. D., & Heckman, T. M. 1989, ApJ, 344, 613
Fried, J. W., & Illingworth, G. D. 1994, ApJ, 107, 992
Grillmair, C. J., et al. 1994, ApJ, 422, L9
Hernquist, L. 1992, ApJ, 400, 460
———. 1993, ApJ, 409, 548
Hernquist, L., & Barnes, J. E. 1991, Nature, 354, 210
Hui, X., Ford, H., Freeman, K. C., & Dopita, M. 1995, ApJ, 449, 592
Jacoby, G. H., Ciardullo, R., & Ford, H. C. 1990, ApJ, 356, 332
Illingworth, G. D. 1977, ApJ, 218, L43
Malin, D. F. 1979, Nature, 277, 279
Ostriker, J. P. 1980, Comm. Astrophys., 8, 177
Peletier, R. F., Davies, R. L., Illingworth, G. D., Davis, L. E., & Cawson, M. 1990, AJ, 100, 1091
Sandage, A. R., & Tamman, G. A. 1981, A Revised Shapley-Ames Catalogue of Bright Galaxies (Washington: Carnegie Inst. of Washington)
Smith, H. A. 1981, AJ, 86, 998
van der Bergh, S., & Tammann, G. A. 1991, ARA&A, 29, 363
Wagner, S. J., Bender, R., & Moellenhoff, C. 1988, A&A, 195,, L5
Whitmore, B. C., McElroy, B. D., & Schweizer, F. 1987, ApJ, 314, 439
Zurek, W. H., Quinn, P. J., & Salmon, J. K. 1988, ApJ, 330, 519